EXPERIMENTAL STUDIES ON THE SHEAR RESISTANCE OF ORIGINAL COAL-SHALE JOINT

B. Guo[1,2,3*], H. Dong[1], L. Wang[4]

[1]Mining Department, School of Energy Science and Engineering, Henan Polytechnic University, Jiaozuo, China
[2]Collaborative Innovation Center of Coal Work Safety, Jiaozuo, China
[3]Key Laboratory of Safety and High-Efficiency Coal Mining, Anhui University of Science and Technology, Huainan, China
[4]School of Safety Science and Engineering, Henan Polytechnic University, Jiaozuo, China
*Corresponding author: e-mail guobaohua@139.com, tel. +8613949669615

ЕКСПЕРИМЕНТАЛЬНІ ДОСЛІДЖЕННЯ СТІЙКОСТІ НА ЗСУВ ШАРУ ВУГІЛЬНОГО СЛАНЦЮ

Б. Ґуо[1,2,3*], Х. Донг[1], Л. Ванг[4]

[1]Школа енергетики та інженерії, Хенанський політехнічний університет, Цзяоцо, Китай
[2]Спільний інноваційний центр безпеки очисних робіт, Цзяоцо, Китай
[3]Лабораторія техніки безпеки та високої ефективності видобування вугілля, Аньхойський університет науки і технології, Хуайнань, Китай
[4]Школа техніки безпеки та інженерії, Хенанський політехнічний університет, Цзяоцо, Китай
*Відповідальний автор: e-mail guobaohua@139.com, тел. +8613949669615

ABSTRACT

Purpose. Experimental study and theoretical modeling of the shear resistance of original coal-shale joint.

Methods. A two-segment model was developed to describe the shear resistance-shear displacement curves obtained from the direct shear tests of eight coal-shale joints by letting the two segments of the fitting curve pass through the peak point of each curve.

Findings. The two-segment model well describes the shear resistance variation of the coal-shale joints during the shear process, and there exist good relationships between the fitting parameters and the shear testing parameters. The initial slope of the softening part of the shear resistance – shear displacement curve can help to predict whether the coal pillar will burst drastically when it fails. Moreover, the normal displacement was very small in the pre-peak range which indicates that the complete detachment of original coal-shale joint surfaces has not occurred before the peak.

Originality. Direct shear tests were conducted on original coal-shale specimens for the first time, and a two-segment model is developed to describe their shear resistance-shear displacement curves. The initial slope of the softening part of the shear resistance – shear displacement curve is proposed to predict the burst tendency of coal pillar. Different from unbonded rock joints, the detachment of the original coal-shale joint occurs just after the peak.

Practical implications. The conclusions may have some help to understand the shear resistance mechanism of original coal-shale joint and to provide some new ideas of maintaining coal pillar stability.

Keywords: rock mechanics, direct shear test, coal-shale joint, shear resistance, shear dilatancy

1. INTRODUCTION

The coal mass surrounding the gob, roadway or chamber in coal mine may fail statically or dynamically during the transferring process of the abutment pressure. The static failure usually contributes to the shape deformation and area reduction of the roadway section, but the dynamic failure may cause dynamic disasters such as rock/coal burst. The similarity between the static and dynamic failures is that the compressive stress of the coal mass exceeds its corresponding compressive strength. The compressive strength of the coal pillar is related to its shape and structure, and is also controlled by the shear resistance of the joints between roof/floor and coal pillar (Wang, Pan, Sheng, & Ding, 2002; Wang, 2005; Chen & Liu, 2013). For the roof-coal-floor structure, the compressive strength of the coal pillar is high before the failure of the joints but becomes lower after the failure of the joints (Iannacchione, 1990; You & Su, 2004). The bearing capacity of the coal pillar maintain its maximum value for initial intact coal-rock joints and degrade to its minimum value when the

shear resistance of the coal-rock joints decrease to its residual value. The coal pillar breaks if the normal stress is bigger than the maximum bearing capacity of the coal pillar and won't break if the normal stress is less than the minimum bearing capacity of coal pillar. The actual bearing capacity of the coal pillar is between its minimum value and maximum value while the shear resistance of the coal-rock joints in the coal pillar is between its residual and peak values. As the shear resistance of joints degrades to some extent, the bearing capacity of the coal pillar will decrease correspondingly, and the coal pillar will break when the bearing capacity of the coal pillar decreases to be less than the loaded constant normal stress between the minimum and maximum bearing capacities of the coal pillar.

There have been some theoretical and experimental studies on the effects of the shear resistance of rock joints on the failure type of coal pillars. Yue (1992) analyzed the effect of the shear strength between coal mass and the roof/floor on the dynamic hazard of a coal pillar by developing a mechanics model and concluded that the bigger the shear strength of joints was, the higher the bearing capacity of the coal pillar was. He and Zou (1993) found that slipping failure of the joint was liable to occur and correspondingly the stability of coal pillar was worse when the joint was composed of strip coal pillar being arranged along the strike direction and the roof/floor. Hu (1995) found that hard roof could improve the stability of coal pillar while tensile failure occurred easily in coal pillar with soft-weak roof. Lu et al. (2008) studied the effect of the cohesive force of a coal-rock joint on the coal pillar compressive strength by a numerical simulation method. Xie and Fan (2008) established a mechanics model to analyze the effect of the friction between the coal seam and the roof/floor on the width of the plastic zone formed in coal pillar, and concluded that the increment of the joint friction force is beneficial to improve the coal pillar stability. Although the studies reviewed above provide valuable contributions to the effect of the shear resistance of joints on the coal pillar stability, however, none of them has studied the reduction characteristic of the shear resistance of coal-rock joint.

As for the experimental studies on the shear resistance of coal-rock joints, Qi et al. (1998) studied the friction characteristics of rock-rock joint, coal-rock joint and coal-coal joint experimentally to analyze the rock burst mechanism caused by the failure of coal-rock joint. Lu et al. (2007) and Dou et al. (2005) studied experimentally the electromagnetic radiation regularities during the dynamical failure processes of roof-coal-floor combined specimens. Guo et al. (2011) studied experimentally the failure mechanism of coal-rock combined specimens with the joint dipping in different angles and concluded that the compressive strength of the coal-rock combined specimen decreased with increase of the joint dip angle. Zuo et al. (2011) studied the mechanical properties of the coal-rock specimens with two equal-length segments of the rock and the coal and found that the failure mainly happened inside the coal segment no matter under uniaxial compression condition or triaxial compression condition. Besides, Liu et al. (2004) and Li et al. (2005) found that the rock burst proneness of the coal-rock combined specimen increased with the increase of the ratio of rock segment length to coal segment length through experimental study. Although the effect of coal-rock joint on the failure patterns of coal segment was involved in almost all experimental studies reviewed above, most of them always focused on the effect of the ratio of the rock segment length to the coal segment length on the failure pattern of the coal-rock combined specimen and ignored the effect of joint shear failure characteristics on the failure pattern of the coal-rock combined specimen. However, the joint shear failure is a key factor to affect the bearing capacity and failure patterns of a coal pillar, the effect of joint shear failure process on the bearing capacity of the coal-rock combined specimen should be focused on in the studies of stability and rock burst proneness of a coal pillar.

The shear resistance variations of the rock joint during the shear process have been studied by some researchers. Haberfield and Seidel (1990) presented a review of the shear resistance evolution of rock joints in the direct shear process. The shear resistance variation of the cemented (Tian, Chen, Yang, & Yang, 2015) or uncemented (Saiang, Malmgren, & Nordlund, 2005) concrete-rock joints was studied by the direct shear tests and the numerical simulation methods, respectively. Liu et al. (2005) carried out a numerical simulation on the interface friction in the direct shear test, and concluded that the shear dilatancy existed in the dense Distinct Element Method (DEM) sample while the shear shrinkage existed for the loose DEM sample. Roosta et al. (2006) proposed a visco-plastic multilaminate model with the hardening and softening effects taken into account to simulate the shear stress-shear displacement curve and the normal displacement-shear displacement curve of the artificial-jointed specimens under Constant Normal Load (CNL) condition. Asadollahi et al. (Asadollahi, Invernizzi, Addotto, & Tonon, 2010) validated the modified Barton's shear strength model for rock joint by conducting a series of direct shear tests. Ghazvinianet et al. (2009) investigated the effect of roughness and compressive strength of joint walls on the shear behavior of the bedding planes between two different rock types with a high compressive strength difference. Park et al. (2013) proposed a constitutive model to describe the shear behavior of rock joints under Constant Normal Stiffness (CNS) and CNL conditions based on the direct shear test results on tensile fractured rock joints and replicas of tensile joints. He et al. (2014) built a piecewise index model to describe the stress and deformation characteristics of structural planes in rock masses. Irregular artificial saw-tooth joints with different asperity heights were sheared by Zhou et al. (2014) in the laboratory to study the shear behavior of joints under various experimental conditions (e.g. different asperity heights, shear rates, and normal loads). Bahaaddini et al. (2014) studied the direct shear behavior of the rock joints using the particle flow code PFC2D. Mirzaghorbanali et al. (2013) numerically studied the shear strength variation of infilled rock joints under cyclic loading and CNS conditions. Nguyen et al. (2014) presented a new procedure to get deeper insight into the shear behavior of rock joints. Indraratna et al. (2014) proposed a new analytical model to predict the shear behavior of rock joints under CNS conditions by incorporating the effect of the asperities damage.

In summary, the shear resistance of rock joints has been studied to some extent, but fewer studies have been done on the shear resistance of the original coal-shale joints. Thus, direct shear tests were conducted in this paper on the original coal-shale joints using the direct shear apparatus RDS-200 to study the shear failure process of the coal-shale joint. The shear resistance-shear displacement curves obtained from the direct shear tests were then analyzed to develop a theoretical model characterizing the joint shear resistance variation, and various parameters affecting the theoretical model were also discussed.

2. MATERIALS AND METHODS

Eight coal-shale specimens containing original coal-shale joints were used for the shear tests and each specimen was prepared into the cube shape with section size of about 70×70 mm. Figure 1 shows the servo-controlled direct shear testing system RDS-200 used in this study, which was manufactured by Geotechnical Consulting and Test Systems (GTCS). In the direct shear testing apparatus, there are two shear boxes, each of them consists of one circular ring, and the coal-shale specimen is placed in these two rings with sufficient length extending into both the upper and lower rings. Cement is used to fix the specimen in the two rings while plasticine is used to isolate the cements in the upper and lower rings. During the shearing test, the moving upper box moves parallel to the fixed lower box. The shear and normal displacements are measured by LVDTs, and the shear and normal load capacities of the direct shear testing system are 10 and 5 t, respectively. Automatic CNS control mode is used for all specimens except the specimen JSC_8, in which the constant displacement control mode is used. The shear displacement rate is set as 1 mm/min.
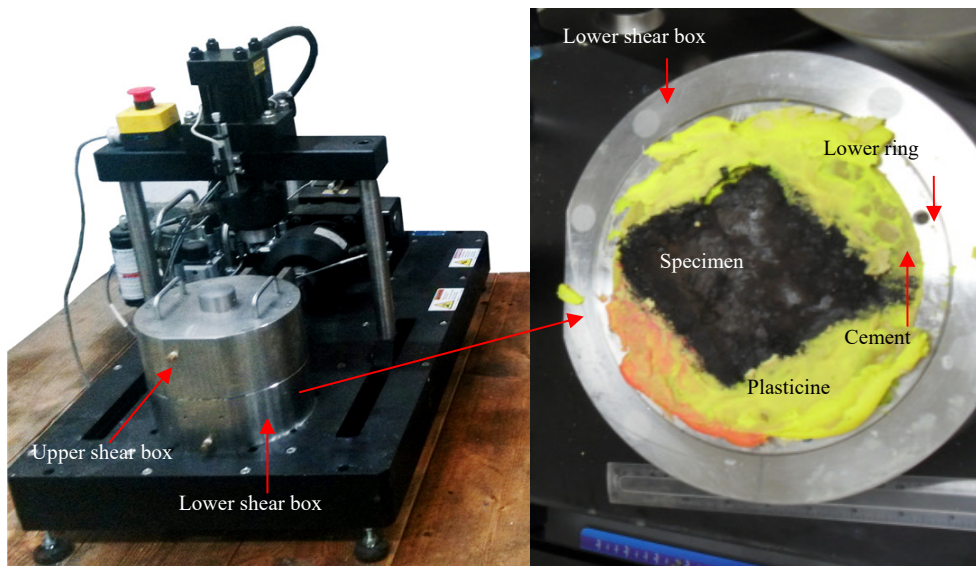

Figure 1. Servo-controlled direct shear testing system RDS-200

3. RESULTS

3.1. The shear resistance-shear displacement curves

Figure 2 illustrates a typical T/N-D_s curve that could be divided into a compression part, a linear part and a yielding part in the pre-peak range while a softening part and a residual part in the post-peak range. The compression part mainly reflects the shear-compression loading characteristics of the coal-shale joint, the linear part mainly reflects the elastic shear deformation characteristics, and the yielding part between yielding point and peak point indicates that the joint surfaces may detach partially from each other. The intersection of the extended regressed straight line of the linear part and the abscissa axis is set as the dividing point between the compression part and the linear part. Correspondingly, the total shearing displacement before the dividing point is defined as D_{sc} while the shear displacement between the dividing point and the peak point is defined as D_{si}. The slope of the line tangent to the initial segment of the softening part is defined as S_{si}, which reflects the drop speed of the shear resistance in the post-peak range.
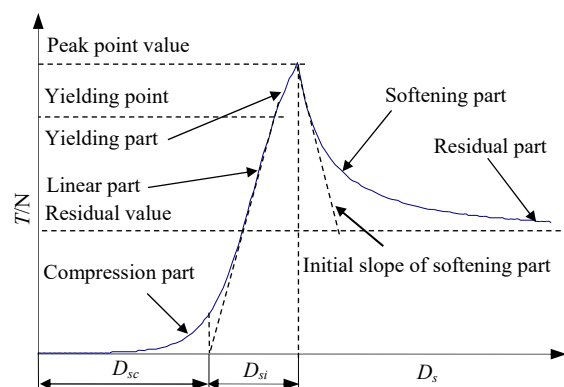

Figure 2. Typical T/N-D$_s$ curve

Figure 3 depicts the shear resistance (the shear load normalized using normal load, i.e. T/N) – shear displacement curves, i.e. the T/N-D_s curves (Lee, Park, & Song, 2014) and the normal displacement-shear displacement curves of the eight specimens. Table 1 summarizes the main physical-mechanical parameters of the eight coal-shale joints.
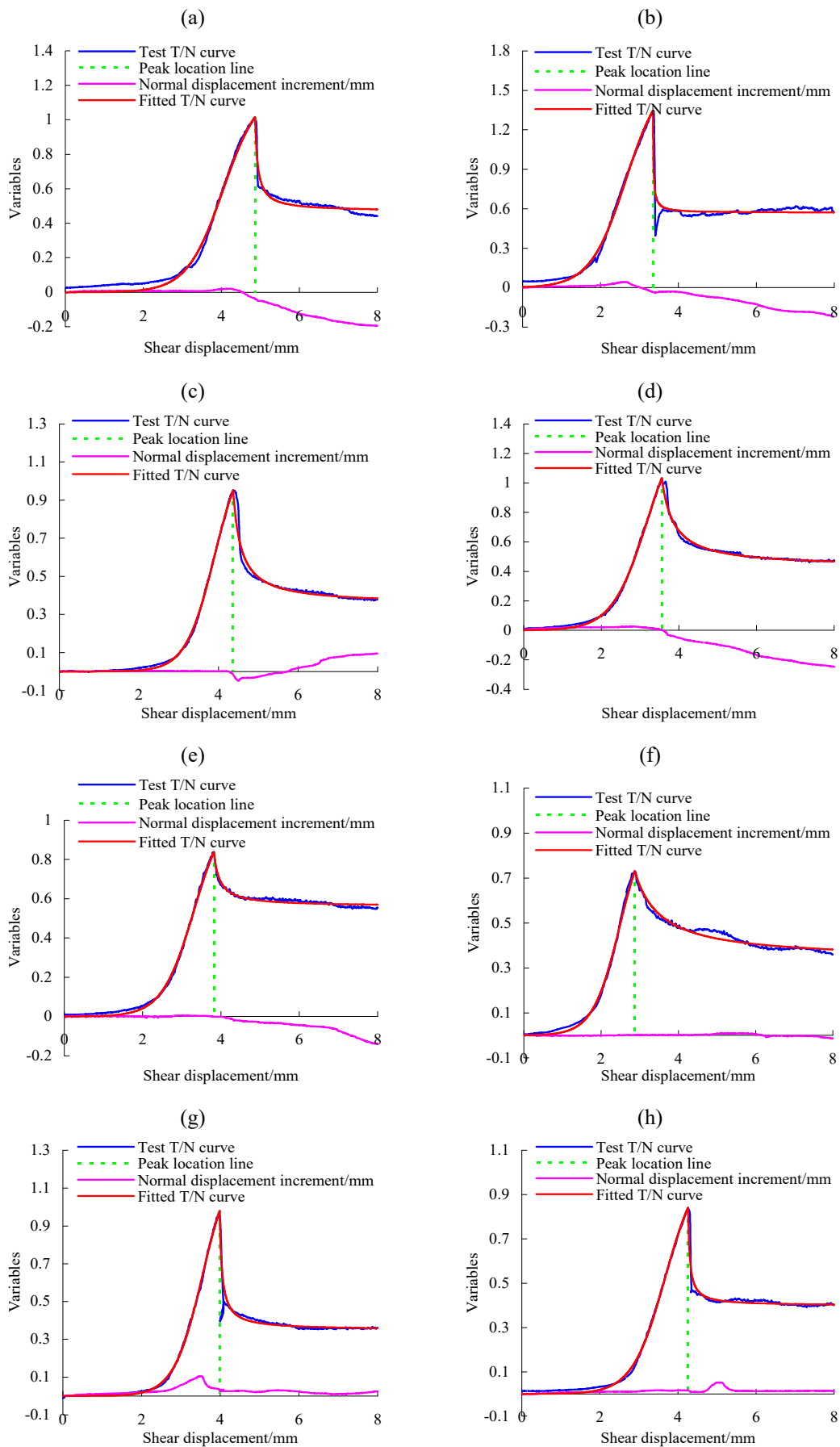
3

***Figure 3.** Relationship between the shear load normalized using the normal load and the shear displacement and that between the normal and shear displacements obtained from the direct shear tests: (a) JSC₁; (b) JSC₂; (c) JSC₃; (d) JSC₄; (e) JSC₅; (f) JSC₆; (g) JSC₇; (h) JSC₈*

Table 1. Main parameters of specimens containing coal-shale joint in direct shear tests

No.	k_n (MPa/mm)	σ_{ni} (MPa)	τ_p (MPa)	σ_{np} (MPa)	D_{sp} (mm)	T/N_p	D_{si} (mm)	S_{si} (mm^{-1})	$T/N_{Ds=8}$
JSC$_1$	0.10	2.50	2.54	2.51	4.86	1.01	1.68	−9.17	0.44
JSC$_2$	0.23	2.50	3.37	2.51	3.35	1.35	1.80	−24.84	0.58
JSC$_3$	0.35	2.50	2.39	2.52	4.37	0.95	1.24	−4.78	0.38
JSC$_4$	0.45	2.50	2.59	2.50	3.56	1.03	1.36	−3.27	0.47
JSC$_5$	0.45	2.50	2.08	2.48	3.82	0.84	1.35	−1.36	0.55
JSC$_6$	0.45	2.50	1.83	2.50	2.87	0.73	1.07	−0.36	0.36
JSC$_7$	6.00	4.30	3.98	4.52	3.99	0.98	1.30	−5.71	0.36
JSC$_8$	*	3.95	3.56	4.24	4.26	0.84	1.53	−10.09	0.40

*under constant normal displacement control mode

From Table 1:

k_n – the normal stiffness, MPa/mm;

σ_{ni} – the initial normal stress, MPa;

τ_p – the shear stress at peak, MPa;

σ_{np} – the normal stress at peak, MPa;

D_{sp} – the shear displacement at peak, mm;

T/N_p – the shear resistance at peak and the value is equal to τ/σ_n;

D_{si} – the shear displacement of the shear resistance increasing, mm;

S_{si} – the initial slope of the softening part, mm^{-1};

$T/N_{Ds=8}$ is the shear resistance at $D_s = 8$ mm.

3.2. The two-equation T/N-D_s model

Both the increasing shear resistance characteristics before the peak point and the decreasing shear resistance characteristics after the peak point of the normalized shear load T/N exist in all non-monotonic T/N-D_s curves. Thus, two fitting functions are used to fit the pre-peak range and post-peak range of the T/N-D_s curves, respectively, and these two fitting curves are required to pass through the peak point of a T/N-D_s curve for each specimen. The fitting function is required to reflect the concave feature of the compression part and the convexity feature of the yielding part, thus the composite function in Equation (1) is chosen to fit the pre-peak range of the T/N-D_s curve:

$$T/N_{bp} = \frac{p_1}{1 + e^{-p_2(D_s - p_3)}}, \tag{1}$$

where:

T/N_{bp} – the normalized shear load T/N before the peak;

D_s – the shear displacement, mm;

p_1 represents the extreme value of T/N_{bp} when the shear displacement is infinite;

p_2 denotes the shear displacement of the joint shear resistance increasing, mm;

p_3 expresses the shear displacement when T/N_{bp} is half of its extreme value, mm.

The hyperbolic function in Equation (2) is chosen to fit the post-peak T/N-D_s curve as follow:

$$T/N_{ap} = \frac{1}{p_4(D_s - p_5)} + p_6, \tag{2}$$

where:

T/N_{ap} – normalized shear load T/N after the peak;

p_4 – reflects the initial slope of the softening part;

p_5 – denotes the right offset distance, mm;

p_6 – represents the residual value of T/N.

Equation (1) and (2) were then used to fit the T/N-D_s curves by requiring both Equation (1) and (2) pass through the peak point (D_{sp}, T/N_p) of each T/N-D_s curve. The regression parameters are summarized into Table 2.

Table 2. Regression parameters

No.	Equation (1)				Equation (2)			
	p_1	p_2	p_3	R^2	p_4	p_5	p_6	R^2
JSC$_1$	1.19	2.16	4.04	0.999	26.75	4.80	0.47	0.87
JSC$_2$	1.64	2.19	2.65	0.999	84.84	3.33	0.57	0.44
JSC$_3$	1.21	2.76	3.90	1.000	8.41	4.17	0.35	0.93
JSC$_4$	1.48	2.21	3.18	0.999	5.42	3.25	0.43	0.97
JSC$_5$	1.08	2.45	3.31	0.998	25.14	3.68	0.56	0.92
JSC$_6$	0.98	2.83	2.48	0.997	3.82	2.21	0.34	0.95
JSC$_7$	1.27	2.74	3.55	0.999	25.67	3.92	0.35	0.95
JSC$_8$	1.04	2.40	3.66	0.999	50.06	4.21	0.40	0.81

While the fitting T/N-D_s curves for the eight specimens are depicted in Figure 2.

It can be seen from Figure 2 and Table 2 that the fitting Equation (1) and (2) well reflect the shape features of the T/N-D_s curves. Specially, the fitting correlation coefficients R^2 for the pre-peak T/N-D_s curves are all larger than 0.99 and those for the post-peak T/N-D_s curves are above 0.8 except that of JSC$_2$. It is also found that the fitting correlation coefficient R^2 for the post-peak T/N-D_s curves increases linearly with the increase of S_{si} but decreases nonlinearly with the increase of p_4 on the whole, as depicted in Figure 4a, b, respectively. That is to say, the

faster the post-peak curve drops, the smaller the fitting correlation coefficient R^2 is. Moreover, Grasselli and Egger (2003) proposed a three-segment constitutive criterion to model the relationship between the shear stress and the shear displacement during the shear failure process of rock joints under CNL conditions. Lee et al. (2014) proposed a two-segment fitting model to describe the shear resistance variation of rock joints. Compared with above two references, from the point of view of fitting effect, the two-equation T/N-D_s model put forward in this paper can also model the shear resistance variation of the coal-shale joint during the direct shear process.
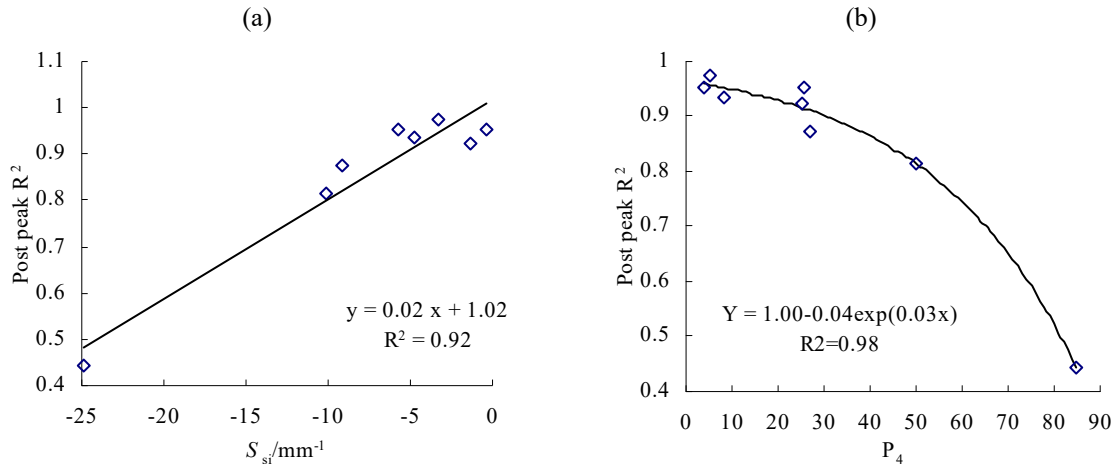
Figure 4. The relationships between post-peak R^2 and S_{si}, p_4: (a) S_{si}; (b) p_4

3.3. The relationships between the regression parameters and test parameters

Figure 5 illustrates the relationships between the fitting parameters $p_1 \sim p_6$ of the two-equation $T/N\text{-}D_s$ model as summarized in Table 2 and the shear testing parameters as listed in Table 1. Simply speaking, p_1 has a positive linear relation with T/N_p (Fig. 5a), p_2 has an inverse linear relation with D_{si} (Fig. 5b), p_3 has a positive linear relationship with D_{sp} (Fig. 5c), p_4 has an inverse linear relation with S_{si} (Fig. 5d), p_5 has a positive linear relation with D_{sp} (Fig. 5e), and p_6 has a positive linear relation with $T/N_{Ds\,=\,8}$ (Fig. 5f). Thus, the

following steps can be taken to use the two-equation $T/N\text{-}D_s$ model in the numerical simulation method to describe the shear resistance of rock joints: (1) the direct shear tests of the rock joint are firstly conducted to obtain T/N_p, D_{si}, D_{sp}, S_{si}, and $T/N_{Ds\,=\,8}$; (2) above testing parameters are then substituted into each equation shown in Figure 5 to determine the fitting parameters $p_1 \sim p_6$; and (3) the fitting parameters $p_1 \sim p_6$ are input into the two-equation $T/N\text{-}D_s$ model embedded in the numerical simulation code to simulate the shear resistance variation of the rock joints in various engineering applications.
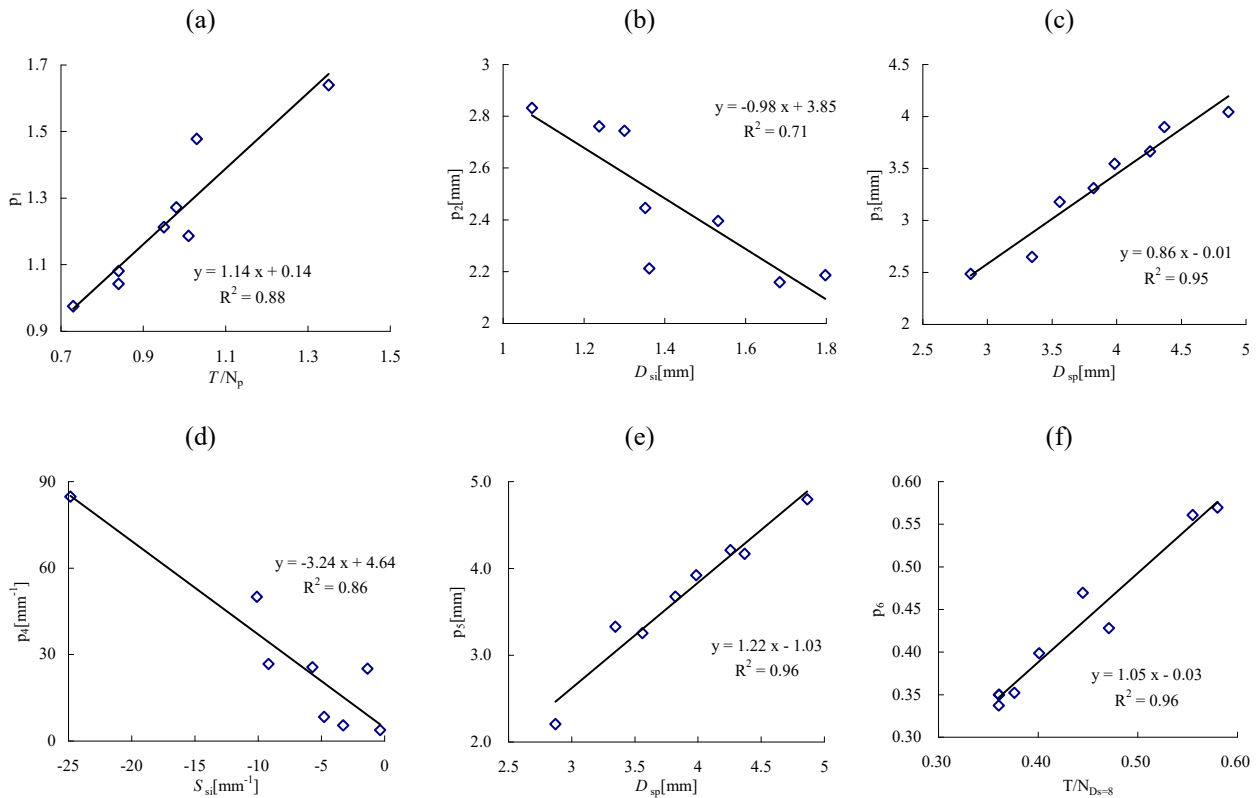

Figure 5. Relationships between the regression parameters in the two-equation $T/N\text{-}D_s$ joint model and the testing parameters from the direct shear test of rock joint: (a) p_1 vs T/N_p; (b) p_2 vs D_{si}; (c) p_3 vs D_{sp}; (d) p_4 vs S_{si}; (e) p_5 vs D_{sp}; (f) p_6 vs $T/N_{Ds\,=\,8}$

4. DISCUSSIONS

4.1. Normal displacement variation during shear process

The normal displacement-shear displacement curves obtained during the shear processes of these eight coal-shale joints are illustrated in Figure 2. Figure 2a – g are obtained from the shear tests under CNS control mode while Figure 2h is under constant normal displacement control mode. As can be seen from Figure 2, with the normalized shear stress approaching the peak, no extensional (negative) normal displacement is observed even some rock joints present the slightly increasing contractive (positive) normal deformation. Therefore, no matter which kind of control modes is adopted in the shear test, the normal displacement in the pre-peak range does not change evidently for original rock joints. Similarly, according to literatures (Lee, Park, & Song, 2014; Oh, Cording, & Moon, 2015), the normal displacement was nearly zero in the pre-peak range during the joint shear process. In order to take the dilation into account, Asadollahi and Tonon (2010) proposed a modified Barton's model which can predict negative compressive dilatancy at small shear displacements; it also shows that negative shear dilatancy may occur before the peak. However, shear shrinkage may exist in both pre-peak and post-peak ranges for open joints under high normal stresses in their direct shear tests.

From Figure 2 it can be also seen that, in the post-peak range, the normal displacement may change significantly, which depends on the roughness of the new detached joint surfaces and the particle sizes of the new generated infilled rock fragments. If the roughness of the new formed joint surfaces is higher, shear dilatancy will occur when the two joint surfaces change into non-matching state during the shear process. Otherwise, shear shrinkage will occur if the infilled rock fragments between the joint surfaces are ground into powder with smaller sizes during the shear process. Combined action of above two phenomena decides the final normal displacement of the coal-shale joint in the direct shear tests.

4.2. The composition evolution of joint shear resistance

The small change of the normal displacement observed in the pre-peak range during the coal-shale joint shearing process may show adequately that the complete detachment of the joint surfaces has not occurred before the peak point. During the shear process, the attached part of the joint surfaces provides shear resistance by static friction (including cohesion between two joint surfaces) while the detached part provides shear resistance by sliding friction. Since the maximum static friction coefficient is greater than the sliding friction coefficient, the shear resistance decreases where the joint surfaces detach, meanwhile the detachment of the joint surfaces in a place leads to the provided static friction increase of its surrounding attached joint surfaces. The shear resistance of the joint is mostly provided by the increasing static friction before the yielding point of the T/N-D_s curve, however, it may be provided by the combination of the static friction between attached joint surfaces and the sliding friction between detached joint surfaces after the yielding point. After the yielding point of the T/N-D_s curve, the static frictions between attached joint surfaces consistently lose and transform into the sliding friction between detached joint surfaces, and the new provided static friction between the surrounding attached joint surfaces gradually increases. However, in the yielding part, the increasing amount of the new provided friction between the surrounding attached joint surfaces is bigger than the decreasing amount of static friction between new detached joint surfaces, which causes the shear resistance increasing continually till the peak. After that, in the softening part, the increasing amount of the new provided static friction between the surrounding attached joint surfaces is lower than the decreasing amount of the static friction between new detached joint surfaces, which causes the shear resistance decreasing in the fast drop form or the gradual decrease form, in which the overall detachment between the two joint surfaces occurs suddenly or gradually, respectively. Finally, all the static friction between the joint surfaces loses and the shear resistance is completely provided by the sliding friction. In the residual part, T/N decreases very slowly with the shear displacement increasing and finally tends to a constant value.

4.3. The relationship between p_4 and coal burst tendency

The confining pressure loaded in triaxial compression test improves the bearing capacity of a cylindrical specimen by limiting the lateral deformation along whole length of the specimen, while the horizontal friction between the testing machine indenter and the specimen ends improves the bearing capacity of the rock specimen by limiting the lateral deformations of two ends, which both improves the bearing capacity of the rock specimen by increasing the normal stress on the potential shear fracture surface. Figure 6 depicts the relationship between the compressive strength and the confining pressure of the specimens obtained by the authors in another study (Guo, 2009). In Figure 6, the point A denotes the axial compressive strength of a rock specimen under the confining pressure of 20 MPa when two ends are fixed horizontally while the point B represents the axial compressive strength of the same rock specimen under the confining pressure of 30 MPa when two ends are totally free horizontally.

The specimen has nearly equal compressive strength although under above different confining pressures, which reveals that the effect of fixing two ends of the specimen horizontally is equivalent to the effect of increasing the confining pressure of 10 MPa on the axial compressive strength of the specimen with two smooth ends. Similarly, the effect of unloading confining pressure may correspond to that of unloading end friction on the axial compressive strength of the specimen. Furthermore, according to the numerical simulation results (Guo, 2009), when the horizontal friction of two ends was set as zero, the softening range of the axial compression stress-strain curve became short and obvious drop occurred after the peak point. Thus, more brittle failure will occur of the rock specimen when the horizontal friction of two ends decreases.
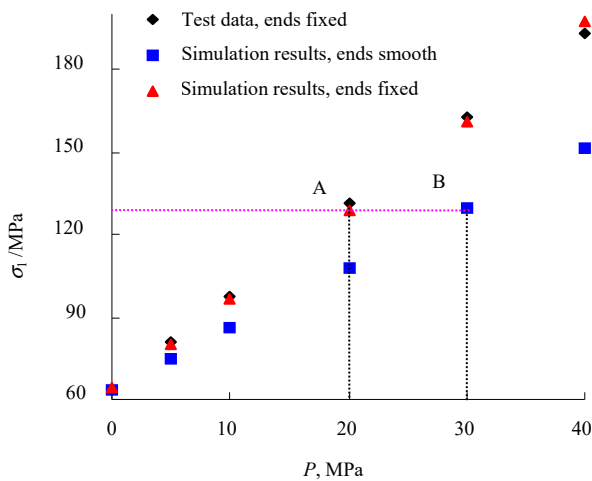
Figure 6. Relationship between strength and confining pressure (Guo, 2009)

Yuan et al. (2006) found that unloading confining pressure rapidly improved the brittleness of rock specimen failure through a numerical simulation method, meanwhile, Wang and Huang (1998) concluded that the larger the unloading ratio of the confining pressure was, the lower the bearing capacity of the rock specimen became, and the lower the initial confining pressure is, the more obvious the brittleness of rock specimen failure was. Therefore, it can be deduced that the reduction rate of the coal-rock joint shear resistance affects the axial compressive strength and the failure type of a coal pillar. The coal pillar failure will be more brittle and prone to burst during its failure when the drop of the coal-rock joint shear resistance is more rapid. As introduced previously, the regression parameter p_4 reflects the drop speed of the softening part of the T/N-D_s curve since it has an inverse linear relation with S_{si}. Thus, the regression parameter p_4 can help to predict whether the coal pillar will burst drastically when it fails, and the coal pillar will burst more intensively when the regression parameter p_4 is bigger.

5. CONCLUSIONS

In this study, the shear resistance characteristics of original coal-shale joints were studied by conducting direct shear tests. The conclusions of this work are summarized as follows:

1. The pre-peak range of the normalized shear stress-displacement T/N-D_s curve can be divided into the compression, linear and yielding parts, while the post-peak range of the T/N-D_s curve can be divided into the softening and residual parts. Two equations including a composite function and a hyperbolic function are used to fit the pre-peak and post-peak ranges of the T/N-D_s curve, respectively. The two-equation T/N-D_s model fitted well the shear stress-displacement curves obtained from the direct shear tests of all eight coal-shale joints under both the CNS and the constant displacement loading conditions with the assumption that the fitting pre-peak and post-peak ranges of the T/N-D_s curve passed through the peak point (D_{sp}, T/N_p). The regression coefficients for the pre-peak range are rather high while those for the post-peak range improve with the increase of S_{si}.

2. The fitting parameters $p_1 \sim p_6$ of the two-equation T/N-D_s model have following relations with the shear testing parameters on the whole: p_1 has a positive linear relation with T/N_p, p_2 has an inverse linear relation with D_{si}, p_3 has a positive linear relationship with D_{sp}, p_4 has an inverse linear relation with S_{si}, p_5 has a positive linear relation with D_{sp}, and p_6 has a positive linear relation with $T/N_{Ds=8}$. The coal pillar will burst more intensively when regression parameter p_4 reflecting the drop speed of the softening part of the T/N-D_s curve is bigger and it can help to predict whether the coal pillar will burst drastically when it fails.

3. The joint normal displacement in the pre-peak range of the T/N-D_s model is not obvious, which indicates that the complete detachment of original coal-shale joint has not occurred before the peak, the whole detachment of the coal-shale joint may occur after the peak.

4. In the pre-yielding range of the two-equation T/N-D_s model, the joint shear resistance of the coal-shale specimen is mainly provided by the static friction between the original attached joint surfaces while it is mainly provided by the sliding friction between the detached joint surfaces in the residual part. In the yielding and softening parts, the shear resistance of the joint is provided by the combination of the static friction between the attached zone of the joint surfaces and the sliding friction between the detached joint surfaces, but the loss amount of the static friction between the attached joint surfaces is lower than the increasing amount of the new provided static friction between the surrounding attached joint surfaces, so that the shear resistance of the coal-shale joint increases gradually till the peak in the yielding part, while in the softening part, the loss amount of the static friction between the attached joint surfaces becomes greater than the increasing amount of the new provided static friction between the surrounding attached joint surfaces, which results in the decrease of the shear resistance.

REFERENCES

Asadollahi, P., Invernizzi, M.C.A., Addotto, S., & Tonon, F. (2010). Experimental Validation of Modified Barton's Model for Rock Fractures. *Rock Mechanics and Rock Engineering, 43*(5), 597-613.
https://doi.org/10.1007/s00603-010-0085-6

Asadollahi, P., & Tonon, F. (2010). Constitutive Model for Rock Fractures: Revisiting Barton's Empirical Model. *Engineering Geology, 113*(1-4), 11-32.
https://doi.org/10.1016/j.enggeo.2010.01.007

Bahaaddini, M., Hagan, P.C., Mitra, R., & Hebblewhite, B.K. (2014). Parametric Study of Smooth Joint Parameters on the Shear Behaviour of Rock Joints. *Rock Mechanics and Rock Engineering, 48*(3), 923-940.
https://doi.org/10.1007/s00603-014-0641-6

Chen, J.Y., & Liu, Z.G. (2013). Numerical Simulation for Failure Process, and Effect of Boundary Restraint of Concrete Specimens in Uniaxial Compression. *Journal of Dalian University of Technology*, (1), 90-96.

Dou, L.M., Tian, J.C., Lu, C.P., Wu, X.R., Mou, Z.L., Zhang, X.T., & Li, Z.H. (2005). Research on Electromagnetic Radiation Rules of Composed Coal-Rock Burst Failure. *Chinese Journal of Rock Mechanics and Engineering*, *24*(19), 3541-3544.

Ghazvinian, A.H., Taghichian, A., Hashemi, M., & Mar'ashi, S.A. (2009). The Shear Behavior of Bedding Planes of Weakness Between Two Different Rock Types with High Strength Difference. *Rock Mechanics and Rock Engineering*, *43*(1), 69-87.
https://doi.org/10.1007/s00603-009-0030-8

Grasselli, G., & Egger, P. (2003). Constitutive Law for the Shear Strength of Rock Joints Based on Three-Dimensional Surface Parameters. *International Journal of Rock Mechanics and Mining Sciences*, *40*(1), 25-40.
https://doi.org/10.1016/s1365-1609(02)00101-6

Guo, B.H. (2009). Numerical Analysis of Size Scale, Inner Hole and End Restraint Effects of Rock Samples. *Chinese Journal of Rock Mechanics and Engineering*, *28*(S2), 3391-3401.

Guo, D.M., Zuo, J.P., Zhang, Y., & Yang, R.S. (2011). Research on Strength, and Failure Mechanism of Deep Coal-Rock Combination Bodies of Different Inclined Angles. *Rock and Soil Mechanics*, *32*(5), 1333-1339.

Haberfield, C.M., & Seidel, J.P. (1990). Some Recent Advances in the Modelling of Soft Rock Joints in Direct Shear. *Geotechnical and Geological Engineering*, *17*(3), 177-195.

He, M.C., & Zou, Y.F. (1993). Analysis of Slide Stability for Strip Pillars. *Hydrogeology and Engineering Geology*, (10), 1-4.

He, Z., Xiong, Z., Hu, Q., & Yang, M. (2014). Analytical and Numerical Solutions for Shear Mechanical Behaviors of Structural Plane. *Journal of Central South University*, *21*(7), 2944-2949.
https://doi.org/10.1007/s11771-014-2261-4

Hu, B.N. (1995). Pillar Stability Analysis in Strip Mining. *Journal of China Coal Society*, (20), 205-210.

Iannacchione, A.T. (1990). The Effects of Roof and Floor Interface Slip on Coal Pillar Behavior. In *Proceedings of the 31st U.S. Symposium* (pp. 153-160). Golden, Colorado: Colorado School of Mines.

Indraratna, B., Thirukumaran, S., Brown, E.T., & Zhu, S.-P. (2014). Modelling the Shear Behaviour of Rock Joints with Asperity Damage Under Constant Normal Stiffness. *Rock Mechanics and Rock Engineering*, *48*(1), 179-195.
https://doi.org/10.1007/s00603-014-0556-2

Lee, Y.K., Park, J.W., & Song, J.J. (2014). Model for the Shear Behavior of Rock Joints Under CNL and CNS Conditions. *International Journal of Rock Mechanics and Mining Sciences*, (70), 252-263.
https://doi.org/10.1016/j.ijrmms.2014.05.005

Li, J.Q., Qi, Q.X., Mao, D.B., & Wang, Y.X. (2005). Discussion on Evaluation Method of Bursting Liability with Composite Model of Coal, and Rock. *Chinese Journal of Rock Mechanics and Engineering*, *24*(S1), 4805-4810.

Liu, B., Yang, R.S., Guo, D.M., & Zhang, D.Z. (2004). Burst-prone Experiments of Coal-Rock Combination at-1100 m Level in Suncun Coal Mine. *Chinese Journal of Rock Mechanics and Engineering*, *23*(14), 2402-2408.

Liu, S.H., Sun, D.A., & Matsuoka, H. (2005). On the Interface Friction in Direct Shear Test. *Computers and Geotechnics*, *32*(5), 317-325.

Lu, C.P., Dou, L.M., & Wu, X.R. (2007). Experimental Research on Rules of Rockburst Tendency Evolution and Acoustic-Electromagnetic Effects of Compound Coal-Rock Samples. *Chinese Journal of Rock Mechanics and Engineering*, *26*(12), 2549-2555.

Lu, J., Ray, A., Morsy, K., & Peng, S. (2008). Effects of Rock/Coal Interface Property on Coal Pillar Strength. In *Proceedings of the 27th International Conference on Ground Control in Mining* (pp. 262-267). Morgantown: West Virginia University.

Mirzaghorbanali, A., Nemcik, J., & Aziz, N. (2013). Effects of Cyclic Loading on the Shear Behaviour of Infilled Rock Joints Under Constant Normal Stiffness Conditions. *Rock Mechanics and Rock Engineering*, *47*(4), 1373-1391.
https://doi.org/10.1007/s00603-013-0452-1

Nguyen, V.-M., Konietzky, H., & Frühwirt, T. (2014). New Methodology to Characterize Shear Behavior of Joints by Combination of Direct Shear Box Testing and Numerical Simulations. *Geotechnical and Geological Engineering*, *32*(4), 829-846.
https://doi.org/10.1007/s10706-014-9761-8

Oh, J., Cording, E.J., & Moon, T. (2015). A Joint Shear Model Incorporating Small-Scale and Large-Scale Irregularities. *International Journal of Rock Mechanics and Mining Sciences*, (76), 78-87.
https://doi.org/10.1016/j.ijrmms.2015.02.011

Park, J.W., Lee, Y.K., Song, J.J., & Choi, B.H. (2013). A Constitutive Model for Shear Behavior of Rock Joints Based on Three-Dimensional Quantification of Joint Roughness. *Rock Mechanics and Rock Engineering*, *46*(6), 1513-1537.
https://doi.org/10.1007/s00603-012-0365-4

Qi, Q.X., Gao, Z.Z., & Wang, S. (1998). The Theory of Rock Burst Led by Structure Failure of Bedded Coal-Rock Mass. *Coal Mining Technology*, (5), 14-17.

Roosta, R.M., Sadaghiani, M.H., Pak, A., & Saleh, Y. (2006). Rock Joint Modeling Using a Visco-Plastic Multilaminate Model at Constant Normal Load Condition. *Geotechnical and Geological Engineering*, *24*(5), 1449-1468.
https://doi.org/10.1007/s10706-005-1217-8

Saiang, D., Malmgren, L., & Nordlund, E. (2005). Laboratory Tests on Shotcrete-Rock Joints in Direct Shear, Tension and Compression. *Rock Mechanics and Rock Engineering*, *38*(4), 275-297.
https://doi.org/10.1007/s00603-005-0055-6

Tian, H.M., Chen, W.Z., Yang, D.S., & Yang, J.P. (2015). Experimental and Numerical Analysis of the Shear Behaviour of Cemented Concrete-Rock Joints. *Rock Mechanics and Rock Engineering*, *48*(1), 213-222.
https://doi.org/10.1007/s00603-014-0560-6

Wang, X.N., & Huang, R.Q. (1998). Analysis of Deformation, and Failure Features Characteristics of Rock Under Unloading Conditions, and Their Effects on Rock Burst. *Mountain Research*, *16*(4), 281-285.

Wang, X.B., Pan, Y.S., Sheng, Q., & Ding, X.L. (2002). Numerical Simulation on Strain Location of End Constraint of Rock Specimen. *Journal of Engineering Geology*, (3), 233-236.

Wang, X.B. (2005). Numerical Simulation of End-Restraint and Failure Process of Three-Dimensional Rock Specimen in Uniaxial Compression. *Journal of Sichuan University*, (2), 28-33.

Xie, Z.B., & Fan, Z.Z. (2008). Research on Stability and Support Design of Strip Coal Pillar. *Coal Science and Technology*, (36), 19-22.

You, M.Q., & Su, C.D. (2004). Effect of Length of Fine and Coarse Crystal Marble Specimens on Uniaxial Compression Tests. *Chinese Journal of Rock Mechanics and Engineering*, (23), 3754-3760.

Yuan, R.F., Li, Y.H., Zhao, X.D., & Yao, X.P. (2006). Analyses of Influence of Unloading Confining Pressure on Failure Modes of Pillar. *Mining Research and Development*, *26*(2), 24-26.

Yue, Z.X. (1992). Mining of Strip Pillar with Rockburst Danger. *Shanxi Coal*, (1), 48-53.

Zhou, H., Meng, F., Zhang, C., Hu, D., Lu, J., & Xu, R. (2014). Investigation of the Acoustic Emission Characteristics of Artificial Saw-Tooth Joints Under Shearing Condition. *Acta Geotechnica*, *11*(4), 925-939.
https://doi.org/10.1007/s11440-014-0359-3

Zuo, J.P., Xie, H.P., Wu, A.M., & Liu, J.F. (2011). Investigation on Failure Characteristics, and Mechanical Behavior of Deep Coal-Rock Single Body, and Combined Body Under Different Confining Pressures. *Chinese Journal of Rock Mechanics and Engineering*, *30*(1), 84-92.

ABSTRACT (IN UKRAINIAN)

Мета. Експериментальне дослідження та теоретичне моделювання опору зсуву початкового шару вуглистого сланцю.

Методика. Розроблено модель для опису кривих опору зсуву й зсувного зміщення, отриманих у результаті випробувань на прямий зсув восьми шарів вуглистого сланцю. Модель включає два сегменти апроксимуючої кривої, що проходять через вищі точки описуваних кривих.

Результати. Запропонована модель достовірно описує зміну опору на зсув шарів вуглистого сланцю в про-процесі зсуву, при цьому визначено наявність тісного зв'язку між параметрами апроксимації та параметрами випробування на зсув. За початковим нахилом кривої в частині ослаблення опору зсуву й зсувного зміщення можна передбачити, чи відбудеться значне руйнування цілика вугілля при його обваленні. Нормальне зміщення є незначним у передпіковому діапазоні, що свідчить про те, що в цей час не відбувається повного відриву поверхонь шару вуглистого сланцю.

Наукова новизна. Випробування на прямий зсув проводилися вперше на зразках початкового вуглистого сланцю. Двохсегментна модель була розроблена спеціально для опису кривих опору зсуву та зсувного зміщення досліджуваних шарів. За початковим нахилом кривої в частині ослаблення опору зсуву й зсувного зміщення можна передбачити характер руйнування цілика. На відміну від незв'язаних шарів породи, відділення початкового шару вуглистого сланцю відбувається після пікових значень досліджуваних кривих.

Практична значимість. Висновки можуть допомогти зрозуміти механізм опору зсуву в первісному шарі вуглистого сланцю й окреслити нові підходи до збереження стабільності вугільного цілика.

Ключові слова: механіка порід, випробування на прямий зсув, шар вуглистого сланцю, опір зсуву, зміна об'єму при зсувній пружній деформації

ABSTRACT (IN RUSSIAN)

Цель. Экспериментальное исследование и теоретическое моделирование сопротивления сдвигу первоначального слоя углистого сланца.

Методика. Разработана модель для описания кривых сопротивления сдвигу и сдвигового смещения, полученных в результате испытаний на прямой сдвиг восьми слоев углистого сланца. Модель включает два сегмента аппроксимирующей кривой которые проходят через высшие точки описываемых кривых.

Результаты. Предлагаемая модель достоверно описывает изменение сопротивления на сдвиг слоев углистого сланца в процессе сдвига, при этом определено наличие тесной связи между параметрами аппроксимации и параметрами испытания на сдвиг. По начальному наклону кривой в части ослабления сопротивления сдвигу и сдвигового смещения можно предсказать, произойдет ли значительное разрушение целика угля при его обрушении. Нормальное смещение незначительно в предпиковом диапазоне, что свидетельствует о том, что в это время не происходит полного отрыва поверхностей слоя углистого сланца.

Научная новизна. Испытания на прямой сдвиг проводились впервые на образцах первоначального углистого сланца. Двухсегментная модель была разработана специально для описания кривых сопротивления сдвигу и сдвигового смещения исследуемых слоев. По начальному наклону кривой в части ослабления сопротивления сдвигу и сдвигового смещения можно предсказать характер разрушения целика. В отличие от несвязанных слоев породы, отделение первоначального слоя углистого сланца происходит после пиковых значений исследуемых кривых.

Практическая значимость. Выводы могут помочь понять механизм сопротивления сдвигу в первоначальном слое углистого сланца и обозначить новые подходы к сохранению стабильности угольного целика.

Ключевые слова: механика пород, испытания на прямой сдвиг, слой углистого сланца, сопротивление сдвигу, изменение объема при сдвиговой упругой деформации

ABOUT AUTHORS

Baohua Guo, Doctor of Philosophy, Associate Professor of the Mining Department, School of Energy Science and Engineering, Henan Polytechnic University, Century Road 2001, Jiaozuo, 454000, Henan Province, China. E-mail: guobaohua@139.com

Hangyu Dong, Postgraduate of the Mining Department, School of Energy Science and Engineering, Henan Polytechnic University, Century Road 2001, Jiaozuo, 454000, Henan Province, China. E-mail: 1468122262@qq.com

Long Wang, PhD Student of the School of Safety Science and Engineering, Henan Polytechnic University, Century Road 2001, Jiaozuo, 454000, Henan Province, China. E-mail: 1029709455@qq.com